

Studying radiation of a white dwarf star falling on a black hole

MAREK NIKOŁAJUK ¹, TOMASZ KARPIUK ¹, LORENZO DUCCI ^{2,3} AND MIROSLAW BREWCZYK ¹

¹*Faculty of Physics, University of Białystok, ul. K. Ciołkowskiego 1L, 15-245 Białystok, Poland*

²*Department of Astronomy, University of Geneva, Chemin d'Ecogia 16, CH-1290 Versoix, Switzerland*

³*Institut für Astronomie und Astrophysik, Kepler Center for Astro and Particle Physics, Eberhard Karls Universität, Sand 1, 72076 Tübingen, Germany*

ABSTRACT

We investigate electromagnetic and gravitational radiation generated during a process of the tidal stripping of a white dwarf star circulating a black hole. We model a white dwarf star by a Bose-Fermi droplet and use the quantum hydrodynamic equations to simulate evolution of a black hole-white dwarf binary system. While going through the periastron, the white dwarf loses a small fraction of its mass. The mass falling onto a black hole is a source of powerful electromagnetic and gravitational radiation. Bursts of ultraluminous radiation are flared at each periastron passage. This resembles the recurrent flaring of X-ray sources discovered recently by Irwin *et al.* Gravitational energy bursts occur mainly through emission at very low frequencies. The accretion disc, formed due to stripping of a white dwarf, starts at some point to contribute continuously to radiation of both electromagnetic and gravitational types.

Keywords: Ultraviolet astronomy(1736) — Interdisciplinary astronomy(804)

1. INTRODUCTION

It is very hard to detect black hole-white dwarf binaries. However, based on known population of white dwarfs, predicted population of black holes, and several possible mechanisms for binaries formation it is expected that such systems exist (Tutukov & Fedorova 2007).

In X-ray data search of nearby galaxies NGC 4636 and NGC 5128 uncovers two sources of ultraluminous X-ray flares from sources not associated with the galactic centres (Irwin *et al.* 2016). All these X-ray bursts have similar rise time, which is less than one minute and the decay time of about an hour. The first source flared once, with an estimated peak X-ray luminosity of $9 \times 10^{40} \text{ erg s}^{-1}$, while the second flared five times and it was ~ 10 times weaker. Prior to and after the flare, a 0.3-10 keV luminosity of the first source was of $7.9 \times 10^{38} \text{ erg s}^{-1}$ and $4 \times 10^{37} \text{ erg s}^{-1}$ in the case of the second source.

Sivakoff *et al.* (2005) reported on another similar X-ray source in the elliptical galaxy NGC 4697 which showed two flares, and more recently, Tiengo *et al.*

(2022) reported a recurrent flaring activity from an ultra-luminous X-ray source in a globular cluster in the galaxy NGC 4472. The properties of these sources are difficult to reconcile with those of better known Galactic accreting X-ray sources, such as the type I and II bursts observed in some low-mass X-ray binaries and beamed emission from stellar mass black holes (Irwin *et al.* 2016; see, however, Sivakoff *et al.* 2005; Maccarone 2005). Therefore, it has been proposed that they might constitute a new type of fast transients Irwin *et al.* (2016). An explanation of observed X-ray bursts as originating from a tidal stripping of a white dwarf (WD) circulating an intermediate-mass black hole has been proposed (Krolik & Piran 2011; Shen 2019; Karpiuk *et al.* 2021; Tiengo *et al.* 2022). Recently two other papers (Miniutti *et al.* 2019; Arcodia *et al.* 2021) reported data showing sequences of quasi-periodic highly energetic X-ray eruptions, with possible explanation that they might be driven by the disruption of a compact object orbiting a supermassive black hole (Arcodia *et al.* 2021; Liu *et al.* 2023).

In this article we study the dynamics of a model white dwarf star in the field of a black hole (BH). The tidal stripping of the WD by the BH causes radiation which is at the centre of our attention. We propose to model a

cold white dwarf star by the Bose-Fermi droplet consisting of ultracold bosonic and fermionic atoms. Such systems have been recently considered theoretically (Rakshit et al. 2019a,b; Karpiuk et al. 2020) and should be possibly realized experimentally. An atomic Bose-Fermi droplet exists because some forces driving system's components counteract with each other. The one is attraction between bosons and fermions. When it is strong enough then the fermion-mediated interactions between bosons make them to be effectively attractive and the whole system becomes unstable due to collapse. The counteracting force is related to quantum pressure of fermionic component. It acts against the collapse of atomic Bose-Fermi droplet just like the pressure of degenerate electrons prohibits the gravitational collapse and stabilize, to some extent, a white dwarf star. The white dwarfs, in fact, very slowly evolve towards an ultimate equilibrium state of the black dwarf. Similarly, the Bose-Fermi droplets are finally stabilized by the action of higher order quantum corrections to the interatomic forces (Rakshit et al. 2019a,b).

An idea of using cold atomic gases as quantum simulators of systems otherwise inaccessible is already well established and sounds in accordance with an old proposition given by Feynman (1982, 1986). For example, this idea has been applied to study a quantum phase transition from a superfluid to a Mott insulator by using a gas of ultracold rubidium atoms in an optical lattice (Greiner et al. 2002) and to investigate critical phenomena near continuous phase transitions (Hung et al. 2011). A two-dimensional caesium atoms' superfluid was quenched to higher interparticle interactions to observe the Sakharov oscillations, which were predicted to occur at the inflation era of the early Universe and are responsible for detected fluctuating cosmic microwave background (Hung et al. 2013). Recently, the Hawking temperature of an analogue black hole was measured experimentally in agreement with the Hawking's theory (Muñoz de Nova et al. 2019). An analogue fluid black hole was created in the Bose-Einstein condensate of rubidium atoms.

The surface temperatures of white dwarf stars, while forming, are of the order of 10^5 K (Goldsbury et al. 2012). Their interior temperatures are much higher, of the order of 10^7 K (Mestel 1952; Shapiro & Teukolsky 1983). They cool down and the surface temperature reaches 2×10^4 K after hundred million years. This temperature falls to 10^4 K over the next billion years (Fontaine et al. 2001). The oldest observed white dwarfs have temperatures of the order of 10^3 K (Kaplan et al. 2014; Kepler et al. 2016).

High densities of WDs ($\lesssim 10^7$ g cm $^{-3}$) lead to very high Fermi temperatures ($\sim 10^{10}$ K). These temperatures are much larger than the initial interior temperatures of WDs ($\sim 10^7$ K, Mestel 1952; Shapiro & Teukolsky 1983). For this reason, electrons can be treated as a gas at zero temperature. For bosonic component, for a WD density of 10^7 g cm $^{-3}$ the critical temperature for Bose-Einstein condensation of ^4He nuclei is 10^6 K. The assumption that the bosonic component becomes condensed, while the white dwarf cools down, seems to be plausible. One could argue against such a scenario based on considerations implying that below a certain value of temperature, the white dwarfs should crystallize (Shapiro & Teukolsky 1983). However, as first discussed in Gabadadze & Rosen (2008a), the crystallization is expected to occur only for white dwarfs composed of carbon, oxygen, and heavier elements. But, due to quantum effects (zero-point oscillations), helium white dwarfs may not solidify. For helium white dwarfs the melting temperature is smaller than the critical temperature for bosonic condensation, therefore there exists a temperature window when charged ^4He nuclei can form a charged condensate (Gabadadze & Rosen 2008b,a; Gabadadze & Pirtskhalava 2009; Mosquera et al. 2010). We are following this line of reasoning and model a white dwarf star as a Bose-Fermi droplet.

In this work, just for simplicity, we consider bosonic and fermionic components of a white dwarf star as gases which have zero initial temperature. This temperature is free and can change during the simulations. Since we study a tidal stripping of a WD circulating an intermediate-mass black hole, some violent dynamics is expected and the falling matter might get heated. Within our description of bosons, so called classical field approximation (for review see Brewczyk et al. 2007), which allows for simultaneous treatment of thermal and condensed particles we can address the question how hot the falling matter is.

The modeling of disruption of a WD by a BH, assuming a white dwarf star is represented by a cosmic Bose-Fermi droplet, was first considered by us in Karpiuk et al. (2021). This work improves on the previous one in some respects: now we study emission of electromagnetic and gravitational waves by WD&BH binary system from the first principles and follow the formation of the accretion disk from the radiation point of view.

We would like to emphasize that our modeling of tidal disruption events of a white dwarf is based on quantum mechanics. Such an attempt is justified and required since cold helium WDs are intrinsically quantum systems and the expectation of appearance of qualitatively new (of quantum nature) phenomena is legitimated.

Then our modeling represents yet another approach to tidal disruption of WDs, complementing already existing reach achievement in the field of dynamics of WDs (for a review of 'smoothed particle hydrodynamics', grid based, and other descriptions see review articles, for example, [Rosswog 2015](#); [Lodato et al. 2020](#)).

2. RADIATION FROM A BLACK HOLE-WHITE DWARF BINARY SYSTEM

Oscillating electric charge radiates electromagnetic waves ([Hertz 1887](#)), in accordance with Maxwell's theory ([Maxwell 1873](#)). Localized charge density can be expanded into multipoles at any time. Since the total charge of a binary system is zero, the lowest order contribution to radiation comes from the oscillating electric dipole moment. The power radiated by a localized but otherwise arbitrary electric dipole moment \mathbf{p} , calculated in the far-field approximation ([Jackson 2021](#); [Griffiths 2024](#)), is

$$P = \frac{2}{3c^3} |\ddot{\mathbf{p}}|^2, \quad (1)$$

where CGS units are used, c is the speed of light, and double dots symbol over the electric dipole moment means the second derivative in time. In the above formula the electric dipole moment \mathbf{p} is given by

$$\mathbf{p} = \int \mathbf{r} \rho_{el}(\mathbf{r}) d^3r, \quad (2)$$

where the charge density is $\rho_{el}(\mathbf{r}) = q_B n_B(\mathbf{r}) - q_F n_F(\mathbf{r})$, while $n_B(\mathbf{r})$ ($n_F(\mathbf{r})$) is the particle number density for bosons (fermions) and q_B and q_F are the electric charges of bosonic and fermionic components' elements building a white dwarf star. Since a white dwarf star is electrically neutral, i.e., $q_B N_B = q_F N_F$ (N_B and N_F are total numbers of bosonic and fermionic particles, respectively), we have

$$\begin{aligned} \mathbf{p} &= q_B N_B \int \mathbf{r} (\bar{n}_B(\mathbf{r}) - \bar{n}_F(\mathbf{r})) d^3r \\ &= q_B N_B \bar{\mathbf{p}}, \end{aligned} \quad (3)$$

where

$$\bar{\mathbf{p}} = \int \mathbf{r} (\bar{n}_B(\mathbf{r}) - \bar{n}_F(\mathbf{r})) d^3r \quad (4)$$

and particle number densities $\bar{n}_B(\mathbf{r})$ and $\bar{n}_F(\mathbf{r})$ are here normalized to one.

The next order contribution to electromagnetic radiation originates from a change of the electric quadrupole moment $Q_{\alpha\beta}$, where indices α and β refer to Cartesian components (contribution coming from a time variation

of the magnetic dipole moment remains of the same order) ([Jackson 2021](#))

$$P = \frac{1}{180c^5} \sum_{\alpha,\beta} (\ddot{Q}_{\alpha\beta})^2, \quad (5)$$

where

$$\begin{aligned} Q_{\alpha\beta} &= \int (3r_\alpha r_\beta - r^2 \delta_{\alpha\beta}) \rho_{el}(\mathbf{r}) d^3r \\ &= q_B N_B \bar{Q}_{\alpha\beta} \\ \bar{Q}_{\alpha\beta} &= \int (3r_\alpha r_\beta - r^2 \delta_{\alpha\beta}) (\bar{n}_B(\mathbf{r}) - \bar{n}_F(\mathbf{r})) d^3r. \end{aligned} \quad (6)$$

The total power radiated by a localized oscillating charge is an incoherent sum of contributions from different multipoles ([Jackson 2021](#)).

Falling mass generates disturbances in the gravitational field and hence becomes the source of gravitational waves travelling in space-time ([Abbott et al. 2016](#)). In the lowest order, the gravitational radiation produced in this way depends on a third time derivative of a mass quadrupole moment $Q_{\alpha\beta}^m$, and is given by a famous Einstein's quadrupole formula ([Maggiore 2008](#); [Jaranowski & Królak 2009](#))

$$P = \frac{G}{45c^5} \sum_{\alpha,\beta} \langle (\ddot{Q}_{\alpha\beta}^m)^2 \rangle, \quad (7)$$

where the average $\langle \cdot \rangle$ is an average over a characteristic time associated with gravitational waves and G is the gravitational constant. The above formula has been indirectly confirmed by measuring the decay of the orbital period with time of the binary pulsar PSR 1913+16 ([Hulse & Taylor 1974, 1975](#); [Taylor et al. 1979](#)). In the case of a black hole-white dwarf binary system one has

$$\begin{aligned} Q_{\alpha\beta}^m &= \int (3r_\alpha r_\beta - r^2 \delta_{\alpha\beta}) (m_B n_B(\mathbf{r}) + m_F n_F(\mathbf{r})) d^3r \\ &= m_B N_B \bar{Q}_{\alpha\beta}^m, \end{aligned} \quad (8)$$

m_B and m_F being the masses of bosonic and fermionic component particles and

$$\begin{aligned} \bar{Q}_{\alpha\beta}^m &= \int (3r_\alpha r_\beta - r^2 \delta_{\alpha\beta}) \left(\bar{n}_B(\mathbf{r}) + \frac{m_F N_F}{m_B N_B} \bar{n}_F(\mathbf{r}) \right) d^3r \\ &\approx \int (3r_\alpha r_\beta - r^2 \delta_{\alpha\beta}) \bar{n}_B(\mathbf{r}) d^3r. \end{aligned} \quad (9)$$

The last term in the upper row of Eq. (9) can be safely neglected since bosonic component mass dominates in the white dwarf stars as well as in the cesium-lithium atomic Bose-Fermi droplets, assumed in our simulations.

3. QUANTUM HYDRODYNAMIC EQUATIONS

We use the formalism of quantum hydrodynamics (Madelung 1927; Frölich 1967; Wong & McDonald 1977; March & Deb 1987) to describe Bose-Fermi mixtures. Such a treatment was already discussed many years ago by Ball *et al.* in the context of the oscillations of electrons in a many-electron atom induced by ultraviolet and soft X-ray photons (Ball *et al.* 1973). They assumed the velocity field of electrons is irrotational. In our study, we follow the same reasoning and apply quantum hydrodynamic equations both for fermionic and bosonic clouds in a droplet.

The quantum hydrodynamic equations for the Bose-Fermi mixture (read Karpiuk *et al.* 2021):

$$\begin{aligned} \frac{\partial n_F}{\partial t} &= -\nabla \cdot (n_F \mathbf{v}_F) \\ m_F \frac{\partial \mathbf{v}_F}{\partial t} &= -\nabla \left(\frac{\delta T}{\delta n_F} + \frac{m_F}{2} \mathbf{v}_F^2 + \frac{\delta E_{BF}}{\delta n_F} \right) \\ \frac{\partial n_B}{\partial t} &= -\nabla \cdot (n_B \mathbf{v}_B) \\ m_B \frac{\partial \mathbf{v}_B}{\partial t} &= -\nabla \left(\frac{\delta E_B}{\delta n_B} + \frac{m_B}{2} \mathbf{v}_B^2 + V_q + \frac{\delta E_{BF}}{\delta n_B} \right), \end{aligned} \quad (10)$$

where the fermionic and bosonic densities ($n_F(\mathbf{r}, t)$, $n_B(\mathbf{r}, t)$) and irrotational velocity fields ($\mathbf{v}_F(\mathbf{r}, t)$, $\mathbf{v}_B(\mathbf{r}, t)$) are used as main variables. Different terms in the right-hand side of Eqs. (10) (the second and the fourth ones) represent various energy components present in the system under consideration. T is the intrinsic kinetic energy of an ideal Fermi gas and is calculated including lowest order gradient correction (Weizsäcker 1935; Kirznits 1957; Oliver & Perdew 1979) and E_{BF} is the boson-fermion interaction energy. E_{BF} includes the mean-field term and a quantum corrections due to quantum fluctuations which is necessary to stabilize the Bose-Fermi droplet (Rakshit *et al.* 2019a). The term E_B describes the interaction between bosons, including the famous Lee-Huang-Yang correction (Lee *et al.* 1957), V_q is related to the bosonic quantum pressure (Madelung 1927). Terms proportional to the square of velocities represent the energies of macroscopic flow of bosonic and fermionic fluids. Detailed formulas are given in Appendix A.

The hydrodynamic equations for fermions can be put in a form of the Schrödinger-like equation by using the inverse Madelung transformation (Dey & Deb 1998; Doms *et al.* 1998; Grochowski *et al.* 2017, 2020). This is just a mathematical transformation which introduces the single complex function instead of density field and velocity field (which represents the potential flow) used in a hydrodynamic description. Both treat-

ments are equivalent provided the velocity field is irrotational. Hence, Eqs. 10 can be turned into coupled Schrödinger-like equations for a condensed Bose field $\psi_B = \sqrt{n_B} \exp(i\phi_B)$ (with $n_B = |\psi_B|^2$ and $\mathbf{v}_B = (\hbar/m_B)\nabla\phi_B$) and a pseudo-wavefunction for fermions $\psi_F = \sqrt{n_F} \exp(i\phi_F)$ (with $n_F = |\psi_F|^2$ and $\mathbf{v}_F = (\hbar/m_F)\nabla\phi_F$): $i\hbar\partial\psi_B/\partial t = H_B^{eff}\psi_B$ and $i\hbar\partial\psi_F/\partial t = H_F^{eff}\psi_F$. The effective nonlinear single-particle Hamiltonians are

$$\begin{aligned} H_B^{eff} &= -\frac{\hbar^2}{2m_B}\nabla^2 + g_B|\psi_B|^2 + \frac{5}{2}C_{LHY}|\psi_B|^3 \\ &+ g_{BF}|\psi_F|^2 + C_{BF}|\psi_F|^{8/3}A(w, \alpha) \\ &+ C_{BF}|\psi_B|^2|\psi_F|^{8/3}\frac{\partial A}{\partial\alpha}\frac{\partial\alpha}{\partial n_B} \end{aligned} \quad (11)$$

and

$$\begin{aligned} H_F^{eff} &= -\frac{\hbar^2}{2m_F}\nabla^2 + (1-\xi)\frac{\hbar^2}{2m_F}\frac{\nabla^2|\psi_F|}{|\psi_F|} \\ &+ \frac{5}{3}\kappa_k|\psi_F|^{4/3} + g_{BF}|\psi_B|^2 \\ &+ \frac{4}{3}C_{BF}|\psi_B|^2|\psi_F|^{2/3}A(w, \alpha) \\ &+ C_{BF}|\psi_B|^2|\psi_F|^{8/3}\frac{\partial A}{\partial\alpha}\frac{\partial\alpha}{\partial n_F} \end{aligned} \quad (12)$$

with all parameters defined in Appendix A. The bosonic wave function and the fermionic pseudo-wave function are normalized to the total number of particles in bosonic and fermionic components, $N_{B,F} = \int d\mathbf{r} |\psi_{B,F}|^2$, respectively.

Next, the Bose-Fermi droplet is placed in the field of an artificial black hole, which is assumed to be a non-rotating black hole described by the Schwarzschild space-time metric. We use further a well-working approximation, given by Paczyński & Wiita (1980), to the potential energy of a test particle moving in the Schwarzschild metric. According to this approximation, the radial part of potential energy is replaced by $V_{PN} = -GM_{BH}/(r - R_S)$, where the Schwarzschild radius is $R_S = 2GM_{BH}/c^2$. The pseudo-Newtonian potential, $V_{PN}(r)$, reproduces correctly the last stable circular orbits. Since it does not depend on the angular momentum, the motion of a test particle can be approximated just as a motion in a three-dimensional space in the field of pseudo-Newtonian potential. Hence, the equations of motion for the Bose-Fermi droplet moving in the field of a fixed black hole can be put in the form

$$\begin{aligned} i\hbar\frac{\partial\psi_B}{\partial t} &= (H_B^{eff} + V_{PN}m_B)\psi_B \\ i\hbar\frac{\partial\psi_F}{\partial t} &= (H_F^{eff} + V_{PN}m_F)\psi_F. \end{aligned} \quad (13)$$

4. SCALING MODEL'S RESULTS TO THE REALM OF ASTRONOMICAL OBJECTS

We solve numerically Eqs. (13) and scale all quantities to the realm of astronomical objects. All quantities used in numerical simulations are given in the code units. A typical scattering length for bosonic atoms a_B ($\simeq 5$ nm) represents the length unit. The mass is expressed in m_B – the mass of bosonic caesium atom ($= 2.21 \times 10^{-25}$ kg). The time unit is given in $(m_B a_B^2)/\hbar$. The last one results from the Schrödinger equation, where $E \propto \hbar^2 \nabla^2 / (2m)$ and therefor time unit is $\propto \hbar/E$. Although the atomic droplet behaviour is simulated, the results can be scaled up to real astronomical sources. To achieve this, let's adopt

$$\begin{aligned} r_{\text{astro}} &= \mathcal{A} r_{\text{num}} [a_B] \\ m_{\text{astro}} &= \mathcal{B} m_{\text{num}} [m_B] \\ t_{\text{real}} &= \mathcal{T} t_{\text{num}} [m_B a_B^2 / \hbar], \end{aligned} \quad (14)$$

where $\mathcal{A}, \mathcal{B}, \mathcal{T}$ are unknown constants. The droplet radius $r_{\text{num}} \simeq 1 \mu\text{m}$ ($= 200 a_B$), and, since the droplet consists of 1460 bosons and 100 fermions in our case, its mass $m_{\text{num}} = 1460 m_B + 100 m_F = 3.23 \times 10^{-22}$ kg (i.e., $m_{\text{num}} = 1464 m_B$). By assuming that $r_{\text{astro}} (= r_{wd})$ and $m_{\text{astro}} (= m_{wd})$ are the typical white dwarf radius and mass ($r_{wd} = 0.01 R_\odot$, $m_{wd} = 1 M_\odot$), we get $\mathcal{A} \approx 7 \times 10^{12}$ and $\mathcal{B} \approx 6 \times 10^{51}$. Hence, after scaling, Eqs. (14), the mass-radius relation for the Bose-Fermi droplet becomes exactly as for a real white dwarf star.

To obtain the coefficient \mathcal{T} we look at how the energy is scaled. Since the unit of energy is given by $m l^2 t^{-2}$, where m, l , and t are the units of mass, length, and time, respectively, we have to multiply the numerical energy by $\mathcal{B} \mathcal{A}^2 \mathcal{T}^{-2}$ to get the astronomical one. Therefore, due to Eqs. (14), one has

$$E_{\text{astro}} = \frac{\mathcal{B} \mathcal{A}^2}{\mathcal{T}^2} E_{\text{num}} [\hbar^2 / (m_B a_B^2)], \quad (15)$$

Continuing the scaling procedure based solely on the properties of a white dwarf star we have

$$E_{\text{astro}}^{WD} = \frac{\mathcal{B} \mathcal{A}^2}{\mathcal{T}^2} \widetilde{E}_{\text{num}}^{BF} \frac{\hbar^2}{m_B a_B^2}, \quad (16)$$

where the tilde symbol means the value of the indicated quantity in the code units (which is $\hbar^2 / (m_B a_B^2)$). Eq. (16) gives the value of the coefficient \mathcal{T} provided the white dwarf (E_{astro}^{WD}) and the Bose-Fermi droplet (E_{num}^{BF}) total energies are known. The total energy of astronomical white dwarf stars ranges from $\sim -10^{44}$ J (near the Chandrasekhar limit) to $\sim -10^{43}$ J. The total energy of the Bose-Fermi droplet used in the simulations is of

the order of -1 in code units. Then Eq. (16) yields $\mathcal{T} \approx 3 \times 10^3$ (for $E_{\text{astro}}^{WD} = -5 \times 10^{43}$ J).

The scaling parameters can also be obtained from the dynamical stripping process of the white dwarf orbiting a black hole, which gives a better insight into the tidal disruption event. Simulations show that the size of the accretion disc is about $200 a_B$ which is $1/4$ of the distance from periastron to the black hole equal to $4 r_{wd}$ (see Sec. 5). Since the radius of the white dwarf star is roughly its Roche lobe at periastron (see equation (1) in Shen 2019) one can write

$$\frac{2 r_{wd}}{4} \left(\frac{M_{BH}}{m_{wd}} \right)^{1/3} = \mathcal{A} 200 a_B, \quad (17)$$

which gives $\mathcal{A} \approx 7 \times 10^{12}$ (for $M_{BH} = 10 M_\odot$, see the following subsection). The value of the outer radius of the accretion disk is calculated in the Appendix B, it is $r_{out} \lesssim 1.3 r_{wd}$ which is very close to the numerical value of r_{wd} . This result indicates that although the atoms in the Bose-Fermi droplet interact via the van der Waals interactions, the dynamics of the droplet can mimic gravitational forces well. This finding highlights the relevance of our computer simulations.

Additionally, accordingly to Shen (2019) (see their equation (3)), the duration of the stripping is roughly given by the internal dynamical time scale $t_{\text{dyn}} \simeq (r_{wd}^3 / (G m_{wd}))^{1/2}$. Then the value of the scaling parameter \mathcal{T} comes from

$$\left(\frac{r_{wd}^3}{G m_{wd}} \right)^{1/2} = \mathcal{T} 10^4 \frac{m_B a_B^2}{\hbar}, \quad (18)$$

where 10^4 is the numerical value of the stripping time (see the next section), and equals $\mathcal{T} \approx 3000$.

4.1. Black hole mass

Scaling, Eq. (15), has strong implications when applied to the gravitational energy of a binary system, leading to

$$G \frac{M_{BH} m_{\text{astro}}}{r_{\text{astro}}} = \frac{\mathcal{B} \mathcal{A}^2}{\mathcal{T}^2} \frac{(\widetilde{GM}_{BH})_{\text{num}} m_{\text{num}} \frac{\hbar^2}{m_B^2 a_B^2}}{r_{\text{num}}}, \quad (19)$$

where $(\widetilde{GM}_{BH})_{\text{num}}$ is the numerical value of the product GM_{BH} which enters the pseudo-Newtonian potential. In numerics, the mass of the black hole, M_{BH} , is encoded in the expression GM_{BH} . However, Eq. (19) makes possible to retrieve M_{BH} via

$$M_{BH} = \frac{\mathcal{A}^3}{\mathcal{T}^2} \frac{(\widetilde{GM}_{BH})_{\text{num}} \frac{\hbar^2}{m_B^2 a_B^2}}{G}. \quad (20)$$

Hence, Eq. (15) allows to find the mass of the black hole which enters the binary system. For $(\widetilde{GM}_{BH})_{\text{num}} \approx 1$, used in simulations, and $\mathcal{T} \approx 3 \times 10^3$ calculated above, Eq. (20) gives the mass of the black hole equal to $M_{BH} \approx 10 M_{\odot}$.

4.2. Scaling the electromagnetic radiation

The dipolar energy radiated during the single event of a tidal stripping is (see Eqs. (1) and (3))

$$\int P_{\text{dip}} dt = \frac{2}{3c^3} (q_B N_B)_{\text{astro}}^2 \left(\int \ddot{\mathbf{p}}^2 dt \right)_{\text{astro}}, \quad (21)$$

where integration is performed over the time of the stripping. Since the unit of $\ddot{\mathbf{p}}^2$ is given by $m l^5 t^{-6}$, the radiated energy, after Eq. (3), scales as

$$\frac{2}{3c^3} \frac{\mathcal{B} \mathcal{A}^5}{\mathcal{T}^5} (q_B N_B)_{\text{num}}^2 \left(\int \ddot{\mathbf{p}}^2 dt \right)_{\text{num}}. \quad (22)$$

The efficiency of conversion of the rest-mass energy of the accreted matter into radiation for Schwarzschild black holes is less than $\eta \approx 0.06$ (Longair 2016). Since the mass stripped off the white dwarf and falling down to the black hole during a single periastron passage is $5 \times 10^{-4} m_{wd}$ (see the next section), the effective charge of bosons is limited by

$$(q_B N_B)_{\text{num}} < \left(\frac{\eta (5 \times 10^{-4} m_{wd}) c^2}{\frac{2}{3c^3} \frac{\mathcal{B} \mathcal{A}^5}{\mathcal{T}^5} \left(\int \ddot{\mathbf{p}}^2 dt \right)_{\text{num}}} \right)^{1/2}. \quad (23)$$

Therefore the dipolar radiation power is bounded by

$$P_{\text{dip}} < \frac{2}{3c^3} \frac{\mathcal{B} \mathcal{A}^5}{\mathcal{T}^6} \text{RHS} \left(\ddot{\mathbf{p}}^2 \right)_{\text{num}}, \quad (24)$$

where RHS is the square of the right hand side of Eq. (23). Since $\int \ddot{\mathbf{p}}^2 dt|_{\text{num}}$ within the first drop (see Fig. 1, upper frame) is $\sim 10^{-12} \hbar^3 / (m_B^3 a_B^4)$ and $\ddot{\mathbf{p}}^2|_{\text{num}} \sim 10^{-15} \hbar^4 / (m_B^4 a_B^6)$ at maxima, the peak dipolar radiation power is estimated as $P_{\text{dip}}^{\text{peak}} \sim 10^{50}$ erg/s.

On the other hand, the luminosity of the flares of electromagnetic radiation originating from the variation of the electric quadrupole moment, Eq. (5), reads

$$P_{\text{quad}} < \frac{1}{180c^5} \frac{\mathcal{B} \mathcal{A}^7}{\mathcal{T}^8} \text{RHS} \left(\sum_{\alpha, \beta} (\ddot{Q}_{\alpha\beta})^2 \right)_{\text{num}}. \quad (25)$$

This is because the unit of $\ddot{Q}_{\alpha\beta}^2$ is $m l^7 t^{-8}$. Since $\sum_{\alpha, \beta} (\ddot{Q}_{\alpha\beta})^2|_{\text{num}} \sim 10^{-14} \hbar^6 / (m_B^6 a_B^8)$ at maxima, the peak quadrupole radiation power for first drops is estimated as $P_{\text{quad}}^{\text{peak}} \sim 10^{49}$ erg/s.

4.3. Scaling the gravitational radiation

The power of gravitational radiation is given by Eq. (7). According to Eq. (8) this radiation scales as

$$\begin{aligned} P_{\text{grav}} &= \frac{G}{45c^5} \left(\sum_{\alpha, \beta} (\ddot{Q}_{\alpha\beta}^m)^2 \right)_{\text{astro}} \\ &= \frac{G}{45c^5} (m_B N_B)_{\text{astro}}^2 \left(\sum_{\alpha, \beta} (\ddot{Q}_{\alpha\beta}^m)^2 \right)_{\text{astro}} \\ &= \frac{G}{45c^5} m_{wd}^2 \frac{\mathcal{A}^4}{\mathcal{T}^6} \left(\sum_{\alpha, \beta} (\ddot{Q}_{\alpha\beta}^m)^2 \Big|_{\text{num}} [\hbar^6 / (m_B^6 a_B^8)] \right). \end{aligned} \quad (26)$$

The scaling factor in the last line in Eq. (26) appears because the unit of $(\ddot{Q}_{\alpha\beta}^m)^2$ is given by $l^4 t^{-6}$. Since $\sum_{\alpha, \beta} (\ddot{Q}_{\alpha\beta}^m)^2|_{\text{num}} \sim 10^{-16} \hbar^6 / (m_B^6 a_B^8)$ at maxima (see the next section), the peak gravitational radiation power is estimated as $P_{\text{grav}}^{\text{peak}} \sim 10^{38}$ erg/s.

5. NUMERICAL RESULTS

We solve numerically Eqs. (13) by split-operator technique (Gawryluk et al. 2018) for trajectories of an atomic white dwarf corresponding to closed eccentric orbits. We consider the Bose-Fermi droplet consisted of ^{133}Cs bosonic and ^6Li fermionic atoms. Such mixtures are studied experimentally nowadays (Pires et al. 2014; De-Salvo et al. 2017, 2019). However, it is not really important which particular atoms are chosen since the mass and the radius of the Bose-Fermi droplet are finally scaled to the mass and size of a real white dwarf star and the total energy of the droplet is of the same order as that of the astronomical WDs. The droplet, consisted of 1460 bosonic and 100 fermionic atoms, is initially located at apastron at some distance (about $7 r_{\text{wd}}$) from the artificial black hole, far away from the horizon. The initial numerical parameters are chosen in such a way that we can follow several revolutions of a white dwarf in an eccentric orbit (with periastron at about $4 r_{\text{wd}}$). Such a task is numerically manageable (i.e., is not too intensive with respect to the computational time) provided the white dwarf is not located extremely far from the black hole. This, on the other hand, means that the period of revolution of a white dwarf around a black hole remains short, in fact it is of the order of ten seconds (see Fig. 1 for $M_{BH} = 10 M_{\odot}$). At each periastron passage a white dwarf is stripped off an approximately (at least within initial few passes) the same mass, which is about 5×10^{-4} of the initial white dwarf mass for a particular orbit discussed below. The dimensionless penetration parameter β ($\equiv r_t / r_{\text{per}}$), where r_t is the tidal radius and r_{per} is the position of the periastron, equals 0.63 in the case of $M_{BH} = 10 M_{\odot}$.

Accelerating localized charged mass is a source of electromagnetic radiation. The lowest order contribution to radiation of a localized charge distribution, which remains neutral, comes from a time-dependent electric dipole moment, Eq. (1). We split the electric dipole moment into parts representing the accretion disk and the matter pulled out of the white dwarf and the white dwarf itself. In our further considerations, we focus on the radiation coming from the accretion disk and the falling matter.

In Fig. 1 we summarize our results for the case of stellar-mass black holes. We show the electromagnetic radiation power of a binary system (with $M_{\text{BH}} = 10 M_{\odot}$) as a function of time, restricting ourselves to two lowest multipoles. We also include the frame (the bottom one) which depicts the incoherent sum of electric dipole and quadrupole contributions. Actually, we also added the contribution from the magnetic dipole term, assuming it is equal to that related to the electric quadrupole one (this assumption seems to be reasonable since both terms appear at the same level of multipole expansion). Ten periastron passages, equally separated in time and lasting each for about 10^4 code units (≈ 1.8 s), can be easily recognized. Clearly, bursts of radiation emerge while a white dwarf is coming through the periastron. Such regular emergence of radiation bursts resembles recurrent flaring of X-ray sources reported recently (Irwin et al. 2016; Miniutti et al. 2019; Arcodia et al. 2021; Tiengo et al. 2022). Since the mass falling to the black hole is huge in our case (it is about $5 \times 10^{-4} m_{\text{wd}}$ which is, in fact, by several orders of magnitude larger than that suggested in Shen (2019) to explain high peak luminosity of observed X-ray flares) the radiation power is enormous, limited by $\sim 10^{50}$ erg/s depending on the conversion efficiency. The amount of dipole radiation exceeds the quadrupole one by an order of magnitude for a stellar-mass black hole case, Fig. 1 (first outburst, in fact, is excessively high, due to a kind of numerical turn-on effect). The total radiation (bottom frame in Fig. 1) understood as the incoherent sum of lowest order multipoles, including the magnetic dipole term, shows regular bursts as well.

Another interesting outcome of numerical simulations is that the accretion disk itself becomes a source of strong electric dipole radiation, see top frame in Fig. 1. Here, the accretion disk activates already after the third passage and becomes dominant at later time. Further properties of dipole radiation can be uncovered by looking at the dipole emission from a binary system in a particular direction. The power of radiation emitted in direction along angle Θ with respect to vector $\hat{\mathbf{p}}$ is

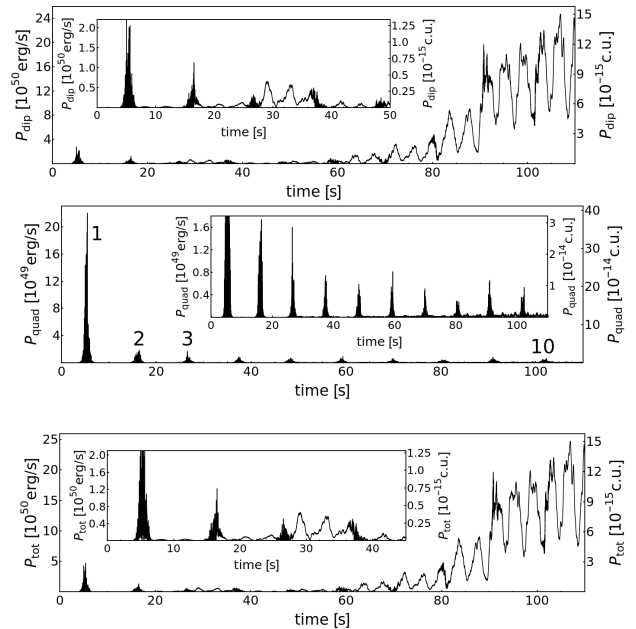


Figure 1. Electromagnetic radiation power of the system of a black hole and a white dwarf as a function of time. Successive frames (from top to bottom) show: electric dipole contribution, electric quadrupole part of radiation (with some passages through periastron marked by numbers, i.e. by 1, 2, 3, and 10), and sum of dipole and twice quadrupole contributions for the case when $M_{\text{BH}}/m_{\text{wd}} = 10$.

(Griffiths 2024)

$$P \sim |\dot{\mathbf{p}}|^2 \sin^2 \Theta. \quad (27)$$

Then the radiation power detected along $\hat{\mathbf{x}}$, $\hat{\mathbf{y}}$, and $\hat{\mathbf{z}}$ directions becomes $P_{x,y,z} \sim \ddot{\mathbf{p}}^2 \left(1 - \ddot{p}_{x,y,z}^2 / \ddot{\mathbf{p}}^2\right)$. Since $p_z = 0$ one has $P_z \sim \ddot{p}^2$ and $P_x + P_y = P_z$. $P_{x,y,z}$ quantities are plotted in Fig. 2 for $M_{\text{BH}}/m_{\text{wd}} = 10$. There is a qualitative difference in the observed dipole radiation depending on the observation angle. Since a charged mass dropped towards an accretion disk still (although for a limited time) orbits a black hole, it can be considered as a rotating electric dipole. Then it can be thought of as a superposition of two dipoles oscillating along x and y axes, respectively, and being out of phase by $\pi/2$. The energy emitted along x and y axes then exhibits a characteristic pattern as a function of time which is $\sim (1 - \cos^2 \omega_d t)$ and $\sim (1 - \sin^2 \omega_d t)$, respectively (see Fig. 2, blue and green curves). Here, ω_d is a frequency of rotating dipole (falling mass on BH) which is higher than the frequency of orbiting white dwarf. Therefore, between two successive periastron passages one observes several oscillations in P_x and P_y , whereas no such behaviour is visible in time-dependence of P_z . The properties of dipole-type radiation can tell us about

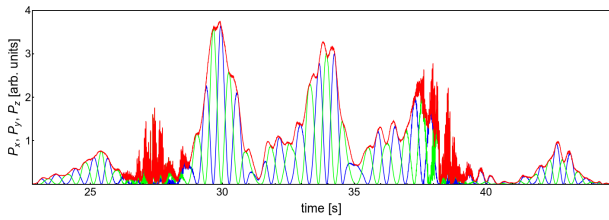


Figure 2. Power of electromagnetic radiation of the system of a black hole and a white dwarf emitted along \hat{x} (blue colour), \hat{y} (green colour), and \hat{z} (red colour) directions as a function of time, showing mainly the time period between the third and fourth periastron passages (see Fig. 1). Curve plotted in red colour is just the sum $P_x + P_y$.

the orientation of the orbital plane of a white dwarf with respect to the Earth. The accretion disc emits much weaker quadrupole-type radiation, see Fig. 1 middle frame. This is understandable since the structure of an accretion disc is mainly that of a rotating electric dipole type.

Formation of an accretion disc is a violent process and it is expected that some part of falling matter becomes hot and its bosonic component can not be still condensed. This is, indeed, the case. The condensate in bosonic part of an accretion disc becomes depleted. We have estimated, by using the classical field approximation (e.g. [Brewczyk et al. 2007](#), for review), how much matter turns into a thermal form. The noncondensed fraction in bosonic matter in accretion disc becomes about 10% for the revolutions below 7th and increase up to 20% for the revolution 9th and successive.

Similar bursts of energy are visible while looking at the gravitational radiation power emitted by a binary black hole-white dwarf system, Fig. 3. However, the amount of energy radiated via gravitational waves remains several orders of magnitudes lower than the energy emitted electromagnetically, compare Figs. 3 and 1. For such a stellar-mass black hole-white dwarf system a peak gravitational-wave luminosity at a periastron passage is of the order of 10^{38} erg/s (see Fig. 3, where instantaneous values, according to Eq. (26), are shown). This is, not surprisingly, much less than the maximum gravitational-wave luminosity detected in GW150914 event, the first observation of gravitational waves from the merger of two stellar-mass black holes ([Abbott et al. 2016](#)), which was $\sim 10^{56}$ erg/s. Two years later LIGO and Virgo detectors made the first observation of a binary neutron star inspiral, known as the signal GW170817 ([Abbott et al. 2017a](#)). The energy radiated via gravitational waves in this event was estimated from below as $0.025M_{\odot}c^2$. Combined with the knowledge of a duration of a gravitational wave signal, which lasted for approximately 100 seconds, leads to av-

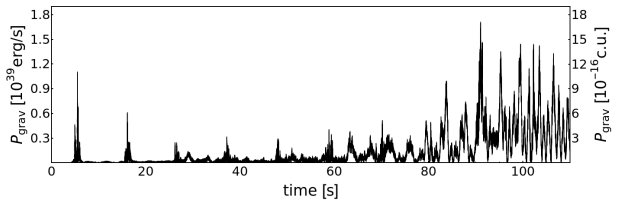


Figure 3. Gravitational radiation power of the system of a black hole and a white dwarf as a function of time for the case $M_{\text{BH}}/m_{\text{wd}} = 10$.

erage radiation power at least of the order of 10^{52} erg/s. Merger of binary neutron stars was followed by a short γ -ray burst GRB 170817A ([Abbott et al. 2017b](#)) located in the same sky position, thus linking the short burst of γ rays to coalescence of neutron stars. The power radiated electromagnetically by GRB 170817A event was estimated as of the order of 10^{46} erg/s, much less than the power radiated via gravitational waves.

For the binary system studied here, with a white dwarf star moving along an eccentric orbit, we observe significant tidal stripping of WD accompanied by emission of electromagnetic and gravitational radiation. The electromagnetic bursts are much stronger than gravitational ones, compare Figs. 1 and 3. An important question concerns the frequencies at which binary system emits its gravitational energy. Here, we are particularly focused on the second periastron passage of a white dwarf, see Fig. 3. The gravitational energy emitted per frequency unit, i.e. power spectral density (PSD), is given by the Fourier transform of gravitational radiation power, Eq. (26),

$$\text{PSD}_{grav} = \left| \mathcal{F} \left[\sqrt{P_{grav}} \right] \right|^2 \quad (28)$$

and is depicted in Fig. 4. It turns out that the energy is mainly radiated at low frequencies, below $\omega/2\pi \approx 1$ Hz, see the inset (more than 95% of total energy is emitted within the range of frequencies $\omega/2\pi < 10$ Hz). Already planned gravitational-wave observatory in space, the Laser Interferometer Space Antenna (LISA), is supposed to work in frequency range covering the one visible in the inset in Fig. 4.

6. CONCLUSIONS

In summary, we have studied the electromagnetic and gravitational radiation coming out of the system of a white dwarf (with mass $\simeq 1M_{\odot}$) orbiting a stellar-mass black hole (with mass $\simeq 10M_{\odot}$). For the trajectory we study, the penetration parameter $\beta = 0.63$. As a model of a white dwarf star, we consider a Bose-Fermi droplet of attractively interacting degenerate atomic bosons and spin-polarized atomic fermions, being initially at zero

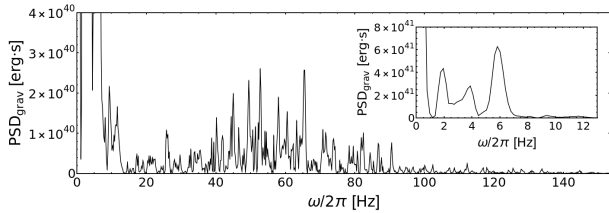


Figure 4. Power spectral density of gravitational waves emitted during the second periastron passage (see Fig. 3) for the case $M_{\text{BH}}/m_{\text{wd}} = 10$. Inset shows PSD for low frequencies, below $\omega/2\pi = 10$ Hz.

temperature. Our quantum hydrodynamics based simulations indeed show that the black hole-white dwarf binary system emits the electromagnetic energy (both in dipole and quadrupole modes) in bursts while crossing the periastron area, with estimated radiation power below $\sim 10^{50}$ erg/s, depending on the radiation efficiency. Such regular high-energy blasts resemble ultraluminous X-ray bursts reported by [Irwin et al. \(2016\)](#). We also

find that the accretion disc, while formed, emits energy mainly via dipole-type radiation. This property can be used to determine the orientation of an orbital plane of a black hole-white dwarf binary system with respect to the observer on the Earth. Our simulations demonstrate that the strong gravitational pulse is emitted at periastron, mainly at very low frequencies. Moreover, it is shown that the binary system becomes a source of nonmonochromatic continuous gravitational radiation as soon as the accretion disc is formed.

T.K. and M.B. acknowledge support from the (Polish) National Science Center Grant no. 2017/25/B/ST2/01943. The publication was produced within the framework of a project subsidized by the Minister of Science under contract no. 2024/WK/03. Part of the results were obtained using computers at the Computer Center of the University of Bialystok.

APPENDIX

A. ENERGY CONTRIBUTIONS

The intrinsic kinetic energy of an ideal Fermi gas is

$$T = \int d\mathbf{r} \left(\kappa_k n_F^{5/3} - \xi \frac{\hbar^2}{8m_F} \frac{(\nabla n_F)^2}{n_F} \right) \quad (\text{A1})$$

with $\kappa_k = (3/10) (6\pi^2)^{2/3} \hbar^2/m_F$ and $\xi = 1/9$ ([Weizsäcker 1935](#); [Kirznits 1957](#); [Oliver & Perdew 1979](#)). The boson-fermion interaction energy is

$$E_{BF} = \int d\mathbf{r} g_{BF} n_B(\mathbf{r}) n_F(\mathbf{r}) + C_{BF} \int d\mathbf{r} n_B n_F^{4/3} A(w, \alpha), \quad (\text{A2})$$

where $w = m_B/m_F$ and $\alpha = 2w(g_B n_B/\varepsilon_F)$ are dimensionless parameters, $C_{BF} = (6\pi^2)^{2/3} \hbar^2 a_{BF}^2/2m_F$, and the function $A(w, \alpha)$ is given in a form of integral ([Viverit & Giorgini 2002](#))

$$A(w, \alpha) = \frac{2(1+w)}{3w} \left(\frac{6}{\pi} \right)^{2/3} \int_0^\infty dk \int_{-1}^+ d\Omega \left[1 - \frac{3k^2(1+w)}{\sqrt{k^2 + \alpha}} \int_0^1 dq q^2 \frac{1 - \Theta(1 - \sqrt{q^2 + k^2 + 2kq\Omega})}{\sqrt{k^2 + \alpha + wk + 2qw\Omega}} \right], \quad (\text{A3})$$

with $\Theta()$ being the step theta-function.

The bosonic quantum pressure term is

$$V_q = -\hbar^2/(2m_B) (\nabla^2 \sqrt{n_B})/\sqrt{n_B}. \quad (\text{A4})$$

The interaction between bosons, including the famous Lee-Huang-Yang correction [Lee et al. \(1957\)](#), is

$$E_B = g_B n_B^2/2 + C_{LHY} \int d\mathbf{r} n_B^{5/2}, \quad (\text{A5})$$

with $C_{LHY} = 64/(15\sqrt{\pi}) g_B a_B^{3/2}$. g_B and g_{BF} appearing in the above energy expressions are coupling constants for contact interactions between atoms ([Pitaevskii & Stringari 2003](#)), with $g_B = 4\pi\hbar^2 a_B/m_B$ and $g_{BF} = 2\pi\hbar^2 a_{BF}/\mu$, where a_B (a_{BF}) is the scattering length corresponding to the boson-boson (boson-fermion) interaction and $\mu = m_B m_F/(m_B + m_F)$ is the reduced mass.

B. SCALING OF THE LENGTH

We saw in Section 4 that \mathcal{A} factor is approximately equal to 7×10^{12} , based on two methods. Let's estimate it again calculating the outer radius of the accretion disk. In a stellar binary system, the outer radius, r_{out} , represents the radius of the first orbit where the accretion disk is formed. The last stable orbit around BH is the innermost stable circular orbit (often called the ISCO). If we assume that the particle in the Kepler orbit at r_{out} has the same angular momentum as it had when it passed through the Lagrange point L_1 (Frank et al. 2002), we get

$$r_{\text{out}} = \frac{X_L^4}{D^3} \frac{M_{BH} + m_{wd}}{M_{BH}}. \quad (\text{B6})$$

D is the distance between BH and WD, $X_L (\simeq D - r_{\text{lobe}})$ is the distance from the BH to the Lagrange point L_1 of the binary system, and r_{lobe} is the Roche lobe around WD. The radius of the WD is slightly larger than or equal to the Roche radius at periastron ($r_{wd} \gtrsim r_{\text{lobe}} \approx 0.8 r_{wd}$, for $M_{BH}/m_{wd} = 10$, see Eq. 2 in Eggleton 1983). Thus, Eq. (B6) can be rewritten as

$$r_{\text{out}} = D \left(1 - \frac{\tilde{r}}{D}\right)^4 (1 + q), \quad (\text{B7})$$

with $q = m_{wd}/M_{BH}$ and $r_{\text{lobe}} < \tilde{r} < r_{wd}$. Next, we will find the distance D on the assumption that it is equal to the radius of the periastron, r_{per} (e.g. Evans et al. 2015; Chen et al. 2023)

$$D \equiv r_{\text{per}} = \beta^{-1} \mu (M_{BH}/m_{wd})^{1/3} r_{wd}, \quad (\text{B8})$$

where β is the dimensionless penetration parameter, and $\mu \simeq 1$. In our case $\beta = 0.63$, $M_{BH} \simeq 10M_{\odot}$, $m_{wd} = 1M_{\odot}$, and $r_{wd} = 0.01R_{\odot}$. Thus, based on Eqs. (B7)-(B8), we get $r_{\text{per}} \simeq 3.4 r_{wd}$ and $0.94 r_{wd} < r_{\text{out}} < 1.3 r_{wd}$. The outer radius of numerical accretion disc is about $200 a_B$. Thus we can write

$$r_{\text{out}} = \mathcal{A} 200 a_B, \quad (\text{B9})$$

which gives $6.6 \times 10^{12} < \mathcal{A} < 9.5 \times 10^{12}$.

REFERENCES

- Abbott, B. P., Abbott, R., Abbott, T. D., et al. 2016, PhRvL, 116, 061102, doi: [10.1103/PhysRevLett.116.061102](https://doi.org/10.1103/PhysRevLett.116.061102)
- . 2017a, PhRvL, 119, 161101, doi: [10.1103/PhysRevLett.119.161101](https://doi.org/10.1103/PhysRevLett.119.161101)
- . 2017b, ApJL, 848, L13, doi: [10.3847/2041-8213/aa920c](https://doi.org/10.3847/2041-8213/aa920c)
- Arcodia, R., Merloni, A., Nandra, K., et al. 2021, Nature, 592, 704, doi: [10.1038/s41586-021-03394-6](https://doi.org/10.1038/s41586-021-03394-6)
- Ball, J. A., Wheeler, J. A., & Firemen, E. L. 1973, Reviews of Modern Physics, 45, 333, doi: [10.1103/RevModPhys.45.333](https://doi.org/10.1103/RevModPhys.45.333)
- Brewczyk, M., Gajda, M., & Rzążewski, K. 2007, Journal of Physics B Atomic Molecular Physics, 40, R1, doi: [10.1088/0953-4075/40/2/R01](https://doi.org/10.1088/0953-4075/40/2/R01)
- Chen, J.-H., Shen, R.-F., & Liu, S.-F. 2023, ApJ, 947, 32, doi: [10.3847/1538-4357/acfbf6](https://doi.org/10.3847/1538-4357/acfbf6)
- DeSalvo, B. J., Patel, K., Cai, G., & Chin, C. 2019, Nature, 568, 61, doi: [10.1038/s41586-019-1055-0](https://doi.org/10.1038/s41586-019-1055-0)
- DeSalvo, B. J., Patel, K., Johansen, J., & Chin, C. 2017, PhRvL, 119, 233401, doi: [10.1103/PhysRevLett.119.233401](https://doi.org/10.1103/PhysRevLett.119.233401)
- Dey, B. K., & Deb, B. M. 1998, Int. J. Quantum Chem., 70, 441
- Domps, A., Reinhard, P. G., & Suraud, E. 1998, PhRvL, 80, 5520, doi: [10.1103/PhysRevLett.80.5520](https://doi.org/10.1103/PhysRevLett.80.5520)
- Eggleton, P. P. 1983, ApJ, 268, 368, doi: [10.1086/160960](https://doi.org/10.1086/160960)
- Evans, C., Laguna, P., & Eracleous, M. 2015, ApJL, 80, L19, doi: [10.1088/2041-8205/805/2/L19](https://doi.org/10.1088/2041-8205/805/2/L19)
- Feynman, R. P. 1982, International Journal of Theoretical Physics, 21, 467, doi: [10.1007/BF02650179](https://doi.org/10.1007/BF02650179)
- . 1986, Foundations of Physics, 16, 507, doi: [10.1007/BF01886518](https://doi.org/10.1007/BF01886518)
- Fontaine, G., Brassard, P., & Bergeron, P. 2001, PASP, 113, 409, doi: [10.1086/319535](https://doi.org/10.1086/319535)
- Frank, J., King, A., & Raine, D. J. 2002, Accretion Power in Astrophysics: Third Edition (Cambridge University Press, United Kingdom)
- Frölich, H. 1967, Physica, 37, 215

- Gabadadze, G., & Pirtskhalava, D. 2009, *JCAP*, 2009, 017, doi: [10.1088/1475-7516/2009/05/017](https://doi.org/10.1088/1475-7516/2009/05/017)
- Gabadadze, G., & Rosen, R. A. 2008a, *JCAP*, 2008, 030, doi: [10.1088/1475-7516/2008/10/030](https://doi.org/10.1088/1475-7516/2008/10/030)
- . 2008b, *Physics Letters B*, 658, 266, doi: [10.1016/j.physletb.2007.08.058](https://doi.org/10.1016/j.physletb.2007.08.058)
- Gawryluk, K., Karpiuk, T., Gajda, M., Rzążewski, K., & Brewczyk, M. 2018, *Int. J. Comput. Math.*, 95, 2143
- Goldsbury, R., Heyl, J., Richer, H. B., et al. 2012, *ApJ*, 760, 78, doi: [10.1088/0004-637X/760/1/78](https://doi.org/10.1088/0004-637X/760/1/78)
- Greiner, M., Mandel, O., Esslinger, T., Hänsch, T. W., & Bloch, I. 2002, *Nature*, 415, 39, doi: [10.1038/415039a](https://doi.org/10.1038/415039a)
- Griffiths, D. J. 2024, *Introduction to electrodynamics* (Cambridge University Press), doi: [10.1017/9781009397735](https://doi.org/10.1017/9781009397735)
- Grochowski, P. T., Karpiuk, T., Brewczyk, M., & Rzążewski, K. 2017, *PhRvL*, 119, 215303, doi: [10.1103/PhysRevLett.119.215303](https://doi.org/10.1103/PhysRevLett.119.215303)
- . 2020, *PhRvL*, 125, 103401, doi: [10.1103/PhysRevLett.125.103401](https://doi.org/10.1103/PhysRevLett.125.103401)
- Hertz, H. 1887, *Annalen der Physik*, 267, 421, doi: [10.1002/andp.18872670707](https://doi.org/10.1002/andp.18872670707)
- Hulse, R. A., & Taylor, J. H. 1974, *ApJL*, 191, L59, doi: [10.1086/181548](https://doi.org/10.1086/181548)
- . 1975, *ApJL*, 195, L51, doi: [10.1086/181708](https://doi.org/10.1086/181708)
- Hung, C.-L., Gurarie, V., & Chin, C. 2013, *Science*, 341, 1213, doi: [10.1126/science.1237557](https://doi.org/10.1126/science.1237557)
- Hung, C.-L., Zhang, X., Gemelke, N., & Chin, C. 2011, *Nature*, 470, 236, doi: [10.1038/nature09722](https://doi.org/10.1038/nature09722)
- Irwin, J. A., Maksym, W. P., Sivakoff, G. R., et al. 2016, *Nature*, 538, 356, doi: [10.1038/nature19822](https://doi.org/10.1038/nature19822)
- Jackson, J. D. 2021, *Classical electrodynamics* (John Wiley & Sons)
- Jaranowski, P., & Królak, A. 2009, *Analysis of Gravitational-Wave Data* (Cambridge University Press, Cambridge)
- Kaplan, D. L., Boyles, J., Dunlap, B. H., et al. 2014, *ApJ*, 789, 119, doi: [10.1088/0004-637X/789/2/119](https://doi.org/10.1088/0004-637X/789/2/119)
- Karpiuk, T., Gajda, M., & Brewczyk, M. 2020, *New Journal of Physics*, 22, 103025, doi: [10.1088/1367-2630/abbcef](https://doi.org/10.1088/1367-2630/abbcef)
- Karpiuk, T., Nikolajuk, M., Gajda, M., & Brewczyk, M. 2021, *Scientific Reports*, 11, 2286, doi: [10.1038/s41598-021-81707-5](https://doi.org/10.1038/s41598-021-81707-5)
- Kepler, S. O., Pelisoli, I., Koester, D., et al. 2016, *MNRAS*, 455, 3413, doi: [10.1093/mnras/stv2526](https://doi.org/10.1093/mnras/stv2526)
- Kirznits, D. A. 1957, *Soviet Physics JETP*, 5, 64
- Krolik, J. H., & Piran, T. 2011, *ApJ*, 743, 134, doi: [10.1088/0004-637X/743/2/134](https://doi.org/10.1088/0004-637X/743/2/134)
- Lee, T. D., Huang, K., & Yang, C. N. 1957, *Physical Review*, 106, 1135, doi: [10.1103/PhysRev.106.1135](https://doi.org/10.1103/PhysRev.106.1135)
- Liu, Z., Malyali, A., Krumpe, M., et al. 2023, *A&A*, 669, A75, doi: [10.1051/0004-6361/202244805](https://doi.org/10.1051/0004-6361/202244805)
- Lodato, G., Cheng, R. M., Bonnerot, C., & Dai, J. L. 2020, *SSRv*, 216, 63, doi: [10.1007/s11214-020-00697-4](https://doi.org/10.1007/s11214-020-00697-4)
- Longair, M. S. 2016, *High Energy Astrophysics* (Cambridge University Press, United Kingdom)
- Maccarone, T. J. 2005, *MNRAS*, 364, 971, doi: [10.1111/j.1365-2966.2005.09623.x](https://doi.org/10.1111/j.1365-2966.2005.09623.x)
- Madelung, E. 1927, *Zeitschrift fur Physik*, 40, 322, doi: [10.1007/BF01400372](https://doi.org/10.1007/BF01400372)
- Maggiore, M. 2008, *Gravitational waves* (Oxford University Press)
- March, N. H., & Deb, B. M. 1987, *The single-particle density in physics and chemistry* (Academic Press, London)
- Maxwell, J. C. 1873, *A treatise on electricity and magnetism* (Clarendon Press)
- Mestel, L. 1952, *MNRAS*, 112, 583, doi: [10.1093/mnras/112.6.583](https://doi.org/10.1093/mnras/112.6.583)
- Miniutti, G., Saxton, R. D., Giustini, M., et al. 2019, *Nature*, 573, 381, doi: [10.1038/s41586-019-1556-x](https://doi.org/10.1038/s41586-019-1556-x)
- Mosquera, M. E., Civitarese, O., Benvenuto, O. G., & de Vito, M. A. 2010, *Physics Letters B*, 683, 119, doi: [10.1016/j.physletb.2009.12.011](https://doi.org/10.1016/j.physletb.2009.12.011)
- Muñoz de Nova, J. R., Golubkov, K., Kolobov, V. I., & Steinhauer, J. 2019, *Nature*, 569, 688, doi: [10.1038/s41586-019-1241-0](https://doi.org/10.1038/s41586-019-1241-0)
- Oliver, G. L., & Perdew, J. P. 1979, *PhRvA*, 20, 397, doi: [10.1103/PhysRevA.20.397](https://doi.org/10.1103/PhysRevA.20.397)
- Paczyński, B., & Wiita, P. J. 1980, *A&A*, 88, 23
- Pires, R., Ulmanis, J., Häfner, S., et al. 2014, *PhRvL*, 112, 250404, doi: [10.1103/PhysRevLett.112.250404](https://doi.org/10.1103/PhysRevLett.112.250404)
- Pitaevskii, L., & Stringari, S. 2003, *Bose-Einstein Condensation* (Oxford University Press)
- Rakshit, D., Karpiuk, T., Brewczyk, M., & Gajda, M. 2019a, *SciPost Physics*, 6, 079, doi: [10.21468/SciPostPhys.6.6.079](https://doi.org/10.21468/SciPostPhys.6.6.079)
- Rakshit, D., Karpiuk, T., Zin, P., et al. 2019b, *New Journal of Physics*, 21, 073027, doi: [10.1088/1367-2630/ab2ce3](https://doi.org/10.1088/1367-2630/ab2ce3)
- Rosswog, S. 2015, *Living Reviews in Computational Astrophysics*, 1, 1, doi: [10.1007/lrca-2015-1](https://doi.org/10.1007/lrca-2015-1)
- Shapiro, S. L., & Teukolsky, S. A. 1983, *Black holes, white dwarfs and neutron stars. The physics of compact objects* (A Wiley-Interscience Publication), doi: [10.1002/9783527617661](https://doi.org/10.1002/9783527617661)
- Shen, R.-F. 2019, *ApJL*, 871, L17, doi: [10.3847/2041-8213/aafc64](https://doi.org/10.3847/2041-8213/aafc64)
- Sivakoff, G. R., Sarazin, C. L., & Jordán, A. 2005, *ApJL*, 624, L17, doi: [10.1086/430374](https://doi.org/10.1086/430374)

Taylor, J. H., Fowler, L. A., & McCulloch, P. M. 1979, Nature, 277, 437, doi: [10.1038/277437a0](https://doi.org/10.1038/277437a0)

Tiengo, A., Esposito, P., Toscani, M., et al. 2022, A&A, 661, A68, doi: [10.1051/0004-6361/202142662](https://doi.org/10.1051/0004-6361/202142662)

Tutukov, A. V., & Fedorova, A. V. 2007, Astronomy Reports, 51, 847, doi: [10.1134/S1063772907100095](https://doi.org/10.1134/S1063772907100095)

Viverit, L., & Giorgini, S. 2002, PhRvA, 66, 063604, doi: [10.1103/PhysRevA.66.063604](https://doi.org/10.1103/PhysRevA.66.063604)

Weizsäcker, C. F. V. 1935, Zeitschrift für Physik, 96, 431, doi: [10.1007/BF01337700](https://doi.org/10.1007/BF01337700)

Wong, C.-Y., & McDonald, J. A. 1977, PhRvC, 16, 1196, doi: [10.1103/PhysRevC.16.1196](https://doi.org/10.1103/PhysRevC.16.1196)